Biology of Reproduction, 2021, 104(3), 611–623
doi:10.1093/biolre/ioaa205
Research Article
Advance Access Publication Date: 9 November 2020

OXFORD

Research Article

Transcriptomic profiling of fetal membranes of mice deficient in biglycan and decorin as a model of preterm birth†

Priyadarshini Pantham[1,2], Don L. Armstrong[2], Jonathan Bodnariuc[2], Owen Haupt[2], Amy Wagoner Johnson[2,3], Lori Underhill[4], Renato V. Iozzo[5], Beatrice E. Lechner[4] and Derek E. Wildman[2,6,*]

[1]Department of Obstetrics, Gynecology, and Reproductive Sciences, University of California San Diego, La Jolla, CA, USA, [2]Carl R. Woese Institute for Genomic Biology, University of Illinois at Urbana-Champaign, Urbana, IL, USA, [3]Department of Mechanical Science and Engineering, University of Illinois at Urbana-Champaign, Urbana, IL, USA, [4]Department of Pediatrics, Women and Infants' Hospital of Rhode Island, Warren Alpert Medical School of Brown University, Providence, RI, USA, [5]Department of Pathology, Anatomy and Cell Biology, Sidney Kimmel Medical College at Thomas Jefferson University, Philadelphia, PA, USA and [6]Genomics Program, College of Public Health, University of South Florida, Tampa, FL, USA

***Correspondence:** College of Public Health, University of South Florida, 3720 Spectrum Blvd., Tampa, FL 33612, USA. Tel: +(813) 974-9775; E-mail: dwildman@usf.edu

†Grant Support: BL is supported by NIH P30 GM114750 and 5P20 GM121298. PP is supported by NIH K99HD096125.

Received 30 March 2020; Revised 9 August 2020; Accepted 6 November 2020

Abstract

Approximately, 25% of all preterm births are due to preterm premature rupture of membranes. Mice deficient in proteoglycans biglycan (*Bgn*) and decorin (*Dcn)* display abnormal fetal membranes and increased incidence of preterm birth. We conducted RNA-Seq to profile fetal membranes and identify molecular pathways that may lead to preterm birth in double knockout (DKO) mice ($Bgn^{-/-}$; $Dcn^{-/-}$) compared to wild-type (WT) at two different gestational stages, E12 and E18 ($n = 3$ in each group). 3264 transcripts were differentially regulated in E18 DKO vs. WT fetal membranes, and 96 transcripts differentially regulated in E12 DKO vs. WT fetal membranes (FDR < 0.05, $\log_2$ FC ≥ 1). Differentially regulated transcripts in E18 DKO fetal membranes were significantly enriched for genes involved in cell cycle regulation, extracellular matrix–receptor interaction, and the complement cascade. Fifty transcripts involved in the cell cycle were altered in E18 DKO fetal membranes (40↓, 10↑, FDR < 0.05), including *p21* and *p57* (↑), and *Tgfb2*, *Smad3*, *CycA*, *Cdk1*, and *Cdk2*(↓). Thirty-one transcripts involved in the complement cascade were altered (11↓, 20↑, FDR < 0.05) in E18 DKO fetal membranes, including *C1q*, *C2*, and *C3* (↑). Differentially expressed genes in the top three molecular pathways (1) showed evidence of negative or purifying selection, and (2) were significantly enriched (Z-score > 10) for transcription factor binding sites for *Nr2f1* at E18. We propose that in DKO mice, cell cycle arrest results in lack of cell proliferation in fetal membranes, inability to contain the growing fetus, and preterm birth.

Summary sentence

We have conducted transcriptomic profiling of fetal membranes from mice deficient in biglycan and decorin and identified molecular pathways of interest.

Key words: amnion, biglycan, decorin, preterm, proteoglycan, fetal membranes.

Introduction

Preterm birth is a leading cause of neonatal mortality and morbidity with a yearly incidence of nearly 12.9 million worldwide [1, 2]. Risk factors for preterm birth include low socio-economic status, infection, ethnicity, stress, trauma, and prior history of preterm birth [3]. Neonates born preterm display a higher risk of developing intraventricular hemorrhage, neurologic impairment, respiratory distress syndrome, and sepsis, amongst other complications, including a greater risk of developing cardiovascular and metabolic disorders in later life. Preterm premature rupture of fetal membranes (PPROM) occurring before 37 weeks of gestation accounts for approximately 25% of all preterm births [4]. In one retrospective study in a Swiss cohort, 60% of all late preterm births (between 34 and 36–37 weeks of gestation) were found to be due to PPROM [5]. Multiple gestations pose significant risk for preterm birth [4], with PPROM occurring in 7.4% of twin pregnancies compared to 3.7% of singleton pregnancies in one study [6].

Human fetal membranes consist of two layers, amnion and chorion. The amnion comprises a layer of epithelial cells and connective tissue. Amnionic mesenchyme is primarily responsible for maintaining tensile strength and consists of a high content of collagen types I and III. The role of collagen in membrane rupture in preterm birth remains uncertain due to contradictory findings from different studies. One study reported a 44% decrease in collagen content in placental tissue from placentas with PPROM compared to spontaneous term placentas [7]. Published evidence regarding the role of extracellular matrix is conflicting, with reduction in hydroxyproline (used as an indicator of collagen content) in placental amnion reported in one study [8], and no changes in another [9]. In addition to collagen, proteoglycans are key structural constituents of the fetal membranes and play key roles in collagen fibrillogenesis and in maintaining tensile strength [10, 11]. Biglycan (BGN) and decorin (DCN) are two such small leucine-rich proteoglycans (SLRPs) that are robustly expressed in the fetal membranes [10, 12]. Moreover, decorin and biglycan are "necessary for maintaining collagen fibril structure, fiber realignment, and mechanical properties of mature tendons" [13]. Decorin interacts with over 60 proteins, including transforming growth factor, matrix constituents and various receptors [14].

The relationship between biglycan, decorin, and collagen in human fetal membranes and their roles in labor have previously been described [12]. Changes in the expression of biglycan, decorin, collagen, and hyaluronan have been described in pre-labor human fetal membranes from caesarean sections compared to post-labor membranes from spontaneous deliveries. Decorin and collagen decrease while biglycan and hyaluronan increase in post-labor amnion compared to pre-labor. Separation of membranes was found to be caused by an increase in hyaluronan. The authors suggest that these biomechanical changes explain the difference in mechanical strength in pre-labor and post-labor fetal membranes [12]. Biglycan and decorin decrease in the human myometrium during term labor [15].

Abnormal secretion of biglycan and decorin due to a mutation in the gene encoding xylosylprotein-4β-galactosyl-transferase-I, an enzyme required for posttranslational glycosylation of these proteoglycans, is the molecular basis of the progeroid type-II variant of the rare inherited genetic connective tissue disorder Ehlers–Danlos syndrome (EDS) [16–18]. EDS is associated with "decreased tensile strength and integrity of skin, joints, and other connective tissue, and infants with EDS have a significantly higher incidence of preterm birth from PPROM compared to their unaffected siblings" [17, 19]. Lechner et al. have previously shown that women who deliver infants due to PPROM display decreased decorin in their fetal membranes [20]. Others have found that a subset of women with recurrent PPROM have undiagnosed connective tissue abnormalities of collagen fibers reminiscent of EDS [21]. Furthermore, preterm delivery with chorioamnionitis is associated with degradation of biglycan and decorin in fetal membranes, indicated by fragmentation of both molecules in affected fetal membranes [22]. These findings have led to the proposition that preterm birth due to PPROM may be associated with underlying abnormalities of the fetal membrane connective tissue [23].

Calmus et al. have previously described a mouse model of preterm birth based on the double knockout of biglycan and decorin ($Bgn^{-/-}$; $Dcn^{-/-}$), a mouse model of EDS. Mice pups lacking both biglycan and decorin are often born prematurely (E15-E18) and display abnormal fetal membrane morphology and signaling [23]. The authors reported that loss of two of the four wild-type (WT) alleles did not alter the length of gestation, but loss of three or four WT alleles resulted in increased risk of preterm birth. Biglycan and decorin may therefore contribute to maintaining full-term gestation in a dose-dependent manner [23]. Decorin-null dams do not present with preterm birth when biglycan is present and functional, and vice versa [23]. Single knockout of decorin alone results in transient temporal abnormalities in collagen fibril ultrastructure and mechanical function in the uterine cervix of mice at E6 [24]. By E12, collagen fibril abnormalities are no longer present, and no mechanical differences were observed in decorin single knockout mice cervices from E12-E18 [24]. Both uterine dystocia (inability of uterine contractions to propel the fetus out the birth canal) and decorin-dependent tissue failure (i.e., breakage under load) are more probable in decorin single knockout mice [25]. Investigation of the effect of single knockout of either biglycan or decorin alone found that the functional SLRP was overexpressed at the protein level in the placenta in a way that compensated for the absence of the missing SLRP, suggesting that compensatory mechanisms may exist between the two proteoglycans [26]. Based on the differences between single knockout of either biglycan or either decorin alone in mice, it has also been suggested that these two SLRPs have non-overlapping functions [27].

There are several different mouse models of preterm birth (reviewed in detail in [28]). Since intrauterine infection is thought to contribute to 25–40% of preterm births in the human [29], mouse models using *Escherichia coli* or lipopolysaccharide (LPS) have been developed to model infection-induced preterm birth [28]. While single knockout of either biglycan or decorin alone does not significantly reduce gestational length, double knockout of biglycan and decorin fetuses causes 43% of dams to deliver before E18 (19.5 days are considered full-length gestation) [23]. While mice in which decorin has been knocked out alone show no adverse pregnancy outcomes these mice do have impaired uterine collagen fibrillogenesis [30]. The demonstrated roles of decorin and/or biglycan to cervical, uterine, and fetal membrane function complicate the ability to attribute compartment-specific contributions to the complex preterm birth and dystocia phenotype in the DKO model. To gain insight into the transcriptomic changes that may be involved in the pathogenesis of preterm birth in this model, we conducted RNA-Seq on fetal membranes of mice deficient in *Bgn* and *Dcn* at embryonic days E12 and E18. We also utilized comparative genomics techniques to examine the evolution of protein coding genes and

regulatory sequences in transcripts involved in overrepresented molecular pathways of interest.

Methods

Mouse husbandry

The biglycan/decorin ($Bgn^{-/-}$; $Dcn^{-/-}$) homozygous double knockout (DKO) mice were bred as described previously. All animal procedures were approved by the Lifespan Institutional Animal Care and Use Committee (IACUC). Briefly, "C3H WT mice were purchased from Jackson Laboratories (Bar Harbor, ME). A $Bgn^{-/-}$ homozygous knockout mutant breeding pair (generated by Marian Young [31]) was a kind gift from Justin Fallon (Brown University). A $Dcn^{+/-}$ heterozygous breeding pair (C57BL/6) [32] was mated to obtain homozygous pups, which were then bred to establish the $Dcn^{-/-}$ homozygous knockout mutant colony. Breeding pairs in which the females were heterozygous for both biglycan and decorin ($Bgn^{+/-}$; $Dcn^{+/-}$), and the males were heterozygous for decorin but homozygous knockouts for biglycan ($Bg^{-/0}$; $Dcn^{+/-}$), given that biglycan is an X-chromosomal gene, were mated to produce offspring, which included $Bgn^{-/-}$; $Dcn^{-/-}$ double knockout pups. A tail biopsy specimen was obtained from each fetal pup of the litter for genotyping. This breeding approach was used as in our experience, double knockout mice do not produce pregnancies. Mice were housed under standard conditions and breeding pairs were set up for mating at 5–7 weeks of age. Breedings were arranged in the evenings, and plugs were checked the following morning and every morning thereafter. The day the plug was observed was defined as embryonic day 0. Pregnant females were euthanized by isoflurane overdose followed by a double thoracotomy. Dams were sacrificed at E12 and E18. $Bgn^{-/-}$; $Dcn^{-/-}$ homozygous double knockout pups bred in this manner have been genotyped as described previously [20, 23, 26, 33]. PCR amplification of *Dcn* produced bands of 161 base pairs (bp) for the WT allele and 238 bp for the knockout allele, and of *Bgn* produced bands of 212 and 310 bp for the WT and knockout alleles, respectively (data not shown)" [23].

RNA extraction from fetal membranes

Transcriptomic analysis was conducted on fetal membranes collected from E12 and E18 in DKO and WT mice. Given that 43% of DKO mice are reported to display preterm birth before E18 [23], it is possible that the E18 fetal membrane samples used in this transcriptome study came from the 57% of DKO mice that did not end up having preterm birth (or more specifically PPROM). However, analysis of fetal membranes at E18 is still informative as it provides insights into the transcriptomic consequences of fetal membrane dysfunction. Fetal membrane tissues were harvested individually from each pup, labeled and flash frozen in liquid nitrogen. The fetal membranes consisted solely of amnion. RNA was extracted from WT and $Bgn^{-/-}$; $Dcn^{-/-}$ homozygous DKO mutant mouse fetal membranes at E12 and E18. Fetal membranes were dissected in 0.1 mol/L phosphate buffered saline, pH 7.4, snap-frozen in liquid nitrogen and stored at −80 °C until RNA extraction was performed. RNA was extracted from mouse fetal membranes collected from E12 WT ($n = 3$), E12 DKO ($n = 3$), E18 WT ($n = 3$), and E18 DKO ($n = 3$) mice. Fetal membranes were ground using a micropestle while maintaining the sample in liquid nitrogen. RNA was extracted using the RNeasy Midi Kit (Qiagen, Valencia, CA) following manufacturer's instructions. Samples were treated with RNase-Free DNase (Qiagen, Valencia, CA) to remove any contaminating DNA. Total RNA concentration was evaluated on a Nanodrop 1000 (Thermo Scientific, Wilmington, DE), and RNA quality was evaluated on an Agilent Bioanalyzer 2100 (Santa Clara, CA). The RNA integrity number (RIN) was 9.6 ± 0.3 for the 12 samples.

RNA-Seq and data processing

RNA-Seq library construction and Illumina sequencing was performed by the Roy J. Carver Biotechnology Institute at the University of Illinois at Urbana-Champaign. Illumina's TruSeq Stranded mRNAseq Sample Prep kit (Illumina, San Diego, CA) was used to prepare RNA-Seq libraries using 2 µg of total RNA and following manufacturer's instructions. cDNA fragments were ∼80–600 bp in length, with an average of 280 bp. Paired-end sequencing was conducted using an Illumina HiSeq 4000 (Illumina, San Diego, CA). Adaptor sequences were trimmed from the 3′-end of the reads using Trimmomatic v0.36 [34]. MultiQC was implemented to assess read quality control [35].

All of the code used to produce the analysis presented in this paper has been previously published [36]. Transcriptomes were aligned against *Mus musculus* reference genome GRCm38 using STAR v2.4.2a [37]. Numbers of reads assigned to features were counted using featureCounts on Subread v1.5.0 [38, 39]. Further analysis was conducted on R v3.3.0 using the edgeR package [40]. Data were filtered to remove features with less than zero counts per million (cpm), and that were not present in at least three samples out of the 12 analyzed. Normalization factors were calculated for each library using the trimmed mean of *M*-values (TMM) method in order to account for differences in library size. Expression values in fragments per kilobase of exon per million reads (FPKM + 1) were calculated from normalized log cpm values. Final FPKM values have been $\log_2$ transformed and changes in transcript expression are represented as $\log_2$-fold change ($\log_2$-FC). Sequencing data are available at Gene Expression Omnibus (GEO, accession number GSE162502).

Identification of differentially expressed transcripts and enrichment of molecular pathways

In order to identify differentially expressed transcripts, we used the limma (Linear Modeling for Microarrays and RNA-Seq Data) package in R [41]. We conducted two pairwise comparisons to compare changes across different gestational ages and knockout conditions: E12 WT vs. E12 DKO, and E18 WT vs. E18 DKO. The Students *t*-test was applied, and *P*-values were corrected for false discovery rate (FDR) using the Benjamini–Hochberg method. Transcripts that were $\log_2$-FC ≥ 1 and FDR < 0.05 were considered for downstream analysis. Enrichment of molecular pathways was conducted using the GOstats package on R, and significantly differentially regulated genes were enriched for Kyoto Encyclopedia of Genes and Genomes (KEGG) pathways with FDR < 0.01 considered significant [42, 43].

Transcription factor motif enrichment

The genes that were differentially regulated in the top three molecular pathways that were enriched in fetal membranes at E18 following DKO were analyzed for enrichment of transcription factor binding sites (TFBS) in *M. musculus* genes using oPOSSUM Version 3.0 [44]. Enrichment for TFBS was conducted using single site analysis on the oPOSSUM program against a background gene set of all 29 347 genes in the oPOSSUM database and the JASPAR vertebrate core profiles. TFBS motif enrichment was determined in conserved regions 10 kb upstream/downstream of the differentially regulated

genes. A conservation cut-off of 0.4, matrix threshold of 85% and minimum specificity of 8-bits was applied [45]. TFBS that were enriched were ranked using Fisher tests and *Z*-scores, and *Z*-score > 10 and Fisher score < 0.01 was considered significant [45, 46].

Molecular evolution of differentially expressed genes in top molecular pathways

In order to determine whether transcriptional changes observed in mouse fetal membranes in response to $Bgn^{-/-}$; $Dcn^{-/-}$ mice can be extrapolated to the human, we investigated whether the genes that were differentially expressed in the top three molecular pathways that were enriched in mouse fetal membranes at E18 underwent purifying (negative) or adaptive (positive) evolution. For each protein coding gene, we calculated the statistic for ω, where $\omega = dN/dS$, or the ratio of the rate of nonsynonymous substitutions per site (dN), to the rate of synonymous substitutions per site (dS). Nonsynonymous nucleotide substitutions result in altered protein sequences, while synonymous substitutions do not. Adaptive evolution is indicated by $\omega > 1$, while $\omega = 1$ indicates neutral evolution, and $\omega < 1$ indicates negative or purifying evolution [47, 48]. For protein coding genes, one to one mouse-human orthologs and dN/dS values were retrieved from *M. musculus* (GRCh38) Ensembl Version 92. Where dN/dS values were not available on Ensembl, they were manually calculated by downloading the protein coding DNA sequences, aligned using MUSCLE, and calculated using PAML (phylogenetic analysis for maximum likelihood) as previously described [49, 50].

Results

Double knockout of biglycan and decorin caused profound transcriptomic changes at E18

Approximately, 770 million 100-bp long paired-end reads were obtained. Quality control analysis indicated that the Phred nucleotide quality score was >30 (indicating 99.9% accuracy of the base call) across the length of the reads. The number of trimmed reads ranged from 2.6 to 3.9 × 10^7 with an average of 85% of reads mapping to the *M. musculus* genome.

Using a cut-off of $\log_2$-FC ≥ 1 and FDR < 0.05, 96 transcripts were differentially regulated when comparing E12 WT to E12 DKO (Figure 1A and Supplementary Table S1). The effect of $Bgn^{-/-}$; $Dcn^{-/-}$ was far more profound at E18, with differential regulation of 3264 transcripts in E18 DKO fetal membranes compared to E18 WT (Figure 1B and Supplementary Table S2). Fifty-nine transcripts were found to overlap when comparing the transcripts that were differentially expressed between E12 WT vs. E12 DKO and E18 WT vs. E18 DKO (Figure 1C).

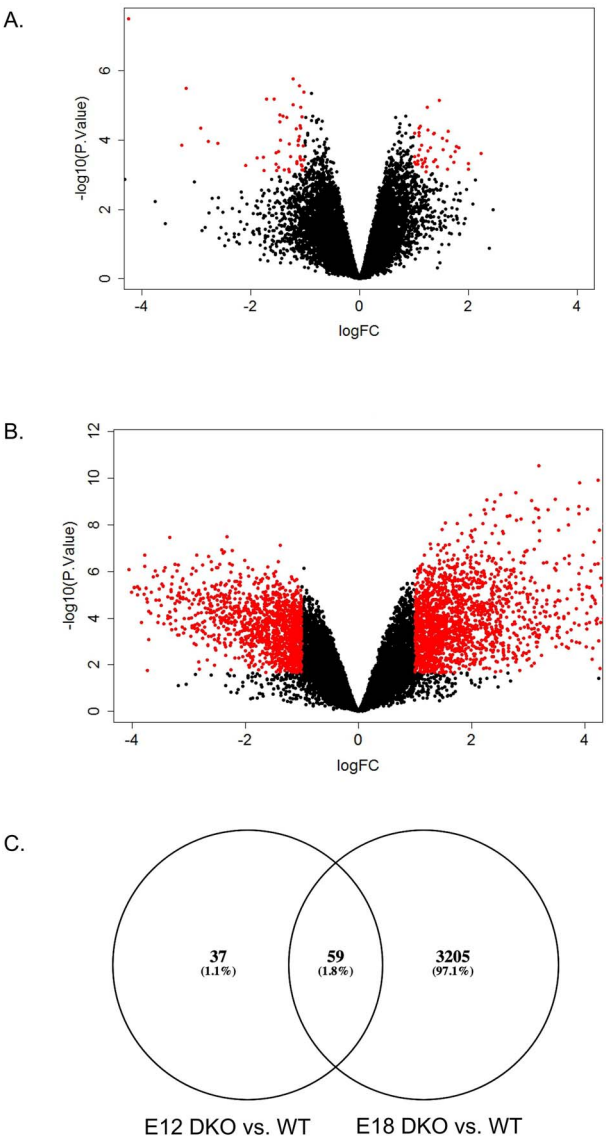

Figure 1. Volcano plots showing the greater number of transcripts that were altered in fetal membranes at E18 following DKO of biglycan and decorin compared to E12. (A) 96 transcripts were differentially expressed (red dots, $\log_2$FC ≥ 1, FDR < 0.05) in E12 WT vs. DKO fetal membranes. (B) 3264 transcripts were differentially expressed (red dots, $\log_2$FC ≥ 1, FDR < 0.05) in E18 WT vs. E18 DKO fetal membranes ($\log_2$FC, log fold-change; WT, wild-type; DKO, double knockout). (C) 59 transcripts were shared between the differentially expressed genes when comparing E12 WT vs. E12 DKO and E18 WT vs. E18 DKO.

Double knockout of biglycan and decorin altered transcripts involved in the cell cycle, ECM interaction, and the complement cascade at E18

The 96 transcripts that were differentially expressed at E12 in mouse fetal membranes due to $Bgn^{-/-}$; $Dcn^{-/-}$ were not significantly enriched for any molecular pathways (FDR > 0.01). The 3264 transcripts that were differentially expressed at E18 in mouse fetal membranes due to $Bgn^{-/-}$; $Dcn^{-/-}$ were significantly enriched for 18 molecular pathways (Table 1). The top three molecular pathways that had the greatest number of genes that were differentially expressed in E18 DKO compared to E18 WT fetal membranes were cell cycle regulation (50 genes), ECM-receptor interaction (36 genes), and the complement and coagulation cascades (31 genes). Fifty differentially expressed transcripts were involved in regulation of the cell cycle, out of which 40 were downregulated and 10 were upregulated (FDR < 0.05) in fetal membranes at E18 in DKO mice compared to WT (Figure 2A). Thirty-six differentially expressed transcripts were involved in ECM-receptor interaction, out of which 13 were downregulated and 23 were upregulated (FDR < 0.05) in fetal membranes at E18 in DKO mice compared to WT (Figure 2B). Thirty-one differentially expressed transcripts were involved in the complement and coagulation cascade (FDR < 0.05), out of which 11 were downregulated and 20 were upregulated (FDR < 0.05) in fetal membranes at E18 in DKO mice compared to WT (Figure 2C).

Table 1. The 18 molecular pathways identified using GOSTATS and the KEGG database, that were significantly enriched (FDR < 0.01) in mouse fetal membranes at E18 in response to DKO of biglycan and decorin, sorted in ascending order of the number of transcripts that were differentially expressed (FDR < 0.01) in each pathway (DKO, double knockout).

KEGGID	No. of genes	Term	FDR
4110	50	Cell cycle	1.81E−09
3030	23	DNA replication	1.81E−09
4512	37	ECM–receptor interaction	4.40E−08
330	26	Arginine and proline metabolism	6.85E−07
4610	31	Complement and coagulation cascades	3.14E−06
260	17	Glycine, serine, and threonine metabolism	8.06E−05
4115	26	p53 signaling pathway	0.000151655
4974	28	Protein digestion and absorption	0.000177236
380	19	Tryptophan metabolism	0.000335247
900	9	Terpenoid backbone biosynthesis	0.000923583
3410	16	Base excision repair	0.000923583
10	22	Glycolysis/gluconeogenesis	0.001066357
1040	12	Biosynthesis of unsaturated fatty acids	0.002061058
3430	11	Mismatch repair	0.002325182
670	10	One carbon pool by folate	0.002535606
620	16	Pyruvate metabolism	0.005350786
71	17	Fatty acid degradation	0.00659291
310	16	Lysine degradation	0.00859972

The 117 transcripts that were differentially expressed in each of the top three molecular pathways are summarized in Table 2.

Enrichment for transcription factor binding sites for Nr2f1

Enrichment for transcription factor motifs using OPOSSUM 3.0 showed that the 117 differentially expressed transcripts in the top three molecular pathways in mouse fetal membranes at E18 following DKO were enriched for regulatory motifs targeted by 116 transcription factors (Supplementary Table S3). Out of the 116 transcription factors, 13 were differentially regulated at E18 in mouse fetal membranes following DKO (Table 3). Out of these, *Nr2f1* (nuclear receptor subfamily 2, group F, member 1) displayed a *Z*-score > 10, with transcription factor motifs in 47 out of the 117 target genes in the top three molecular pathways. *Nr2f1* displayed $\log_2$-FC reduction of 1.03 (FDR = 0.01) in E18 $Bgn^{-/-}$; $Dcn^{-/-}$ DKO mouse fetal membranes compared to E18 WT.

Differentially expressed genes in top three molecular pathways are evolutionarily conserved between mouse and human

In order to determine whether the 117 transcripts that were differentially expressed in mouse fetal membranes at E18 are evolutionarily conserved between mouse and human, we tested for purifying and adaptive selection in differentially expressed transcripts in the top three molecular pathways (Table 2). All of the differentially expressed transcripts involved in regulation of the cell cycle, ECM-receptor interaction, and complement cascade showed evidence of negative or purifying selection, with $\omega < 1$ (Table 2).

Discussion

There are few studies profiling the transcriptomic changes in fetal membranes across gestation, as human fetal membranes are inaccessible prior to delivery [51]. In this report, we have utilized a mouse model, which to our knowledge is the only model of a genetic disruption leading to spontaneous preterm birth in mice, to profile transcriptomic changes across gestation in fetal membranes. We have shown for the first time that double knockout of the genes biglycan and decorin in this mouse model results in: (1) greater transcriptomic changes in the fetal membranes at E18 compared to E12, (2) down-regulation of transcripts associated with cell cycle regulation, (3) Disruption of transcripts associated with ECM-receptor interaction, and (4) upregulation of transcripts associated with complement activation at E18. These findings have important implications for our understanding of the pathophysiology of fetal membrane rupture in preterm birth and can inform efforts to develop effective intervention strategies to prevent preterm birth.

While both humans and mice have discoid, hemochorial placentas, there are some differences in the development of the human and mouse fetal membranes. Human amnion consists of two portions: the thicker placental portion contiguous to the chorionic plate, and the fetal portion contiguous to the umbilical cord and surrounding the fetus [52]. In the mouse, by E7.5, the amnion and chorion separate, and the two membranes are no longer in contact with each other. Rodent amnion is therefore not incorporated in the placenta, and remains a thin, avascular membrane [52, 53]. Despite these differences, mice are the most utilized and studied animal model in investigating mechanisms of preterm birth, especially involving an inflammatory component [54].

Fewer transcripts were altered when comparing the DKO and WT fetal membrane phenotypes at E12 fetal membranes. The majority of transcriptomic changes occurred in fetal membranes at E18 in response to loss of biglycan and decorin, compared to changes between E12 and E18 WT mice (Supplementary Table S4). This suggests that the profound changes in the transcriptomic profile are due to the effect of DKO and not due to temporal changes across gestation alone. In the mouse, E17 until birth (E19–21 in different mouse strains) represents a period of accelerated growth in the mouse and roughly equates to 197–294 gestational days or the third trimester in the human [55–57]. In normal gestation, cells of

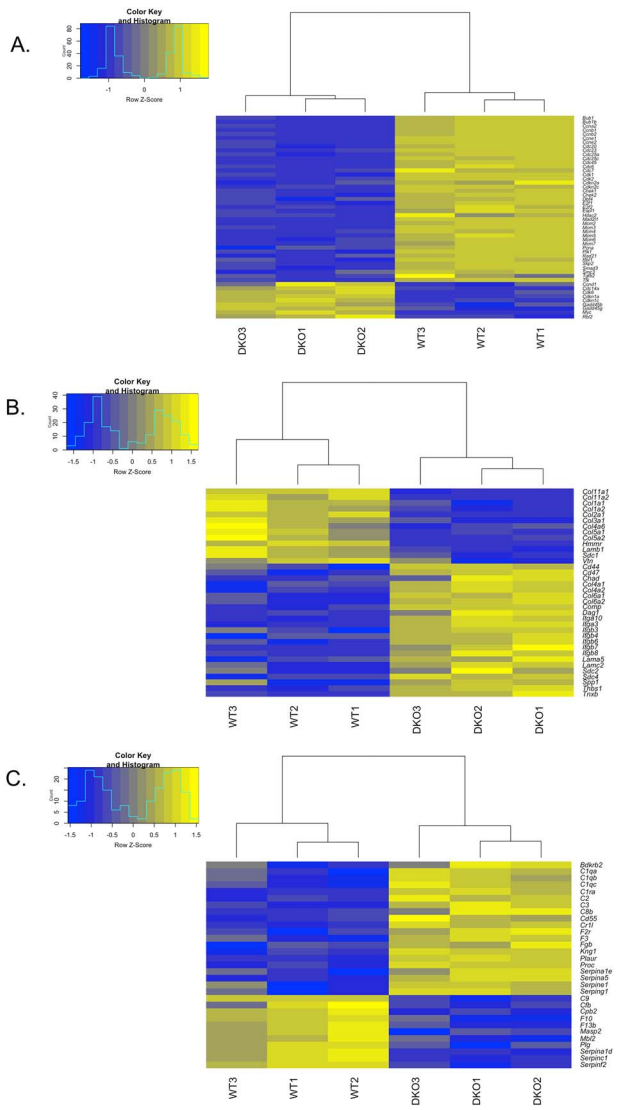

Figure 2. Heatmaps showing the differential expression of transcripts involved in the top three molecular pathways in E18 DKO fetal membranes. Differentially regulated transcripts ($log_2FC \geq 1$, FDR < 0.05) involved in (A) the cell cycle (FDR < 0.01), (B) ECM-receptor interaction, and (C) the complement and coagulation cascade in fetal membranes from *Bgn* $^{-/-}$; *Dcn* $^{-/-}$ mice at E18 (WT, wild-type; DKO, double knockout; Yellow, increase, blue, decrease).

the fetal membranes are likely to undergo rapid proliferation and expansion during this time in order to accommodate the rapidly growing fetuses. In the mouse, E18 may therefore be a crucial point in gestation where these proliferative changes occur. The top molecular pathway with the greatest number of transcripts involved that was dysregulated in E18 fetal membranes from DKO mice was in fact regulation of the cell cycle, in which 50 transcripts were altered. Upregulated transcripts included *p21* and *p57*, and downregulated transcripts included transforming growth factor beta 2 (*Tgfb2*), mothers against decapentaplegic homolog 3 (*Smad3*), cyclin A (*CycA*), cyclin-dependent kinases (*Cdk1*, *Cdk2*), and transcription factor family *E2f1*, and *E2f2*. These transcripts are of interest due to the identification of their dysregulation at the level of protein expression in previous studies investigating the role of biglycan or decorin alone in the cell cycle. Knockout of biglycan alone using siRNA in colon cancer cells causes cell cycle arrest at the G0/G1 phase, mediated by an increase in protein expression of p21, and decreased expression of cyclin A and D1 [58]. Opposingly, ectopic expression of decorin in neoplastic cells derived from various tissue origins including cervical carcinoma, SV40-transformed skin fibroblasts, osteosarcoma, colon carcinoma, prostate adenocarcinoma, melanoma, and different types of leukemia cell lines resulted in retardation of cell growth via induction of endogenous p21 [59]. E2f1 and E2f2 are classically known as transcriptional activators, and are expressed during the cell cycle with maximal levels observed in the late G1 and early S1 phase [60]. E2fs regulate the expression of a number of factors including p21, which in turn functions as a negative feedback loop to limit E2f transcriptional activity.

The proteoglycan cores of biglycan and decorin interact with all isoforms of TGF-β [61], a cytokine that promotes or inhibits cell proliferation in different cell types [62]. Both biglycan and decorin are regulated by TGF-β [63]. Decorin modulates TGF-β activity via a negative feedback mechanism [64]. Biglycan and decorin bind and abrogate the activity of transforming growth factor-β (TGF-β), which in turn signals via Smads to modulate the extracellular matrix [33]. Dysregulated TGF-β-Smad signaling resulting in downstream disruptions in collagens, tissue inhibitors of matrix metalloproteinases (TIMPs), and matrix metalloproteinases (MMPs) has been implicated in the pathogenesis of PPROM in other studies [33]. The TGF-β signaling cascade has previously been investigated in fetal membranes at E12 and E18 following knockout of either biglycan or decorin alone, and has highlighted differential mechanisms of TGF-β signaling at these two time points of gestation in single knockouts [33]. Biglycan stabilizes membranes in a TGF-β-dependent manner late in gestation, while decorin supports membrane remodeling in a TGF-β-dependent manner early during gestation [26]. Knockout of decorin alone in fetal membranes at E18 results in decreased expression of phosphorylated Smad3, a key downstream effector of the TGF-β cascade [33]. Downstream TGF-β signaling may therefore play a key role in cell proliferation in fetal membranes due to this interaction. Although previous evidence suggests a reduction in MMP-8 and MMP-9 expression at the protein level in fetal membranes from *Bgn* or *Dcn* single knockouts at E12 [33], our study did not find differential expression of these MMPs at the transcript level at E12 in DKO fetal membranes. Only MMP-2 and MMP-9 were detectable at the transcript level in E12 fetal membranes, with no significant changes in expression of these transcripts ($log_2FC \geq 1$, FDR ≥ 0.01). This discrepancy in MMP expression between studies may be attributed to the observation that transcript levels are often poorly correlated with protein levels across a wide range of conditions and cell types [65], and the effect of single knockout of either *Bgn* or *Dcn* vs. loss of both *Bgn* and *Dcn*.

The effect of decorin knockout on collagen in connective tissue is well documented in mice. Collagen in *Dcn*$^{-/-}$ mice is clearly variable in shape and size, specifically displaying thick and thin collagen fibrils of irregular sizes while WT mice show almost exclusively thick fibrils [30, 66]. Abnormalities and aberrant patterning are a shared feature in decorin knockouts as well as knockouts for other proteoglycans. Double knockout mice also display a wider range of variation in fetal membrane width than single knockouts [33], analogous to the thick and thin filaments noted above [30]. The collagen-binding activity of decorin decreases in affected births and may contribute to decreased membrane integrity and therefore PPROM in women [22]. In this transcriptomic study, we confirm that double knockout of biglycan and decorin causes disruption in ECM-receptor interactions, since this molecular pathway was significantly

Table 2. The 117 transcripts in the top three molecular pathways that were dysregulated in mouse fetal membranes when comparing E18 WT to DKO of biglycan and decorin (WT, wild-type; DKO, double knockout), and their $\omega = d_N/d_S$ values (d_N, rate of nonsynonymous substitutions; d_S, rate of synonymous nucleotide substitutions).

ENSEMBL ID	Gene symbol	Gene name	Log_2 Fold-change (DKO vs. WT)	FDR	d_N/d_S
Cell cycle: KEGG ID 4110					
ENSMUSG00000027379	*Bub1*	Mitotic checkpoint serine/threonine-protein kinase BUB1	-2.83	0.0004	0.37
ENSMUSG00000040084	*Bub1b*	Mitotic checkpoint serine/threonine-protein kinase BUB1 beta	-3.04	0.0002	0.23
ENSMUSG00000027715	*Ccna2*	Cyclin-A2	-3.18	0.0002	0.18
ENSMUSG00000041431	*Ccnb1*	G2/mitotic-specific cyclin-B1	-3.16	0.0003	0.11
ENSMUSG00000032218	*Ccnb2*	G2/mitotic-specific cyclin-B2	-3.96	0.0002	0.11
ENSMUSG00000070348	*Ccnd1*	G1/S-specific cyclin-D1	1.16	0.0212	0.03
ENSMUSG00000002068	*Ccne1*	G1/S-specific cyclin-E1	-2.43	0.0005	0.12
ENSMUSG00000028212	*Ccne2*	G1/S-specific cyclin-E2	-1.15	0.0018	0.11
ENSMUSG00000033502	*Cdc14a*	Dual specificity protein phosphatase CDC14A	2.31	0.0000	0.18
ENSMUSG00000006398	*Cdc20*	Cell division cycle protein 20 homolog	-3.79	0.0003	0.05
ENSMUSG00000024370	*Cdc23*	Cell division cycle protein 23 homolog	-1.23	0.0008	0.05
ENSMUSG00000032477	*Cdc25a*	M-phase inducer phosphatase 1	-1.02	0.0005	0.21
ENSMUSG00000044201	*Cdc25c*	M-phase inducer phosphatase 3	-2.38	0.0017	0.45
ENSMUSG00000000028	*Cdc45*	Cell division control protein 45 homolog	-2.12	0.0008	0.08
ENSMUSG00000017499	*Cdc6*	Cell division control protein 6 homolog	-1.51	0.0015	0.26
ENSMUSG00000029283	*Cdc7*	Cell division cycle 7-related protein kinase	-1.26	0.0038	0.22
ENSMUSG00000019942	*Cdk1*	Cyclin-dependent kinase 1	-3.52	0.0003	0.02
ENSMUSG00000025358	*Cdk2*	Cyclin-dependent kinase 2	-1.14	0.0008	0.02
ENSMUSG00000040274	*Cdk6*	Cyclin-dependent kinase 6	1.71	0.0099	0.05
ENSMUSG00000023067	*Cdkn1a*	Cyclin-dependent kinase inhibitor 1	2.44	0.0012	0.16
ENSMUSG00000037664	*Cdkn1c*	Cyclin-dependent kinase inhibitor 1C	2.18	0.0000	0.33
ENSMUSG00000044303	*Cdkn2a*	Tumor suppressor ARF	-1.19	0.0226	0.18
ENSMUSG00000028551	*Cdkn2c*	Cyclin-dependent kinase 4 inhibitor C	-2.40	0.0000	0.15
ENSMUSG00000032113	*Chek1*	Serine/threonine-protein kinase Chk1	-1.62	0.0041	0.14
ENSMUSG00000029521	*Chek2*	Serine/threonine-protein kinase Chk2	-1.26	0.0009	0.15
ENSMUSG00000002297	*Dbf4*	Protein DBF4 homolog A	-1.48	0.0008	0.36
ENSMUSG00000027490	*E2f1*	Transcription factor E2F1	-2.11	0.0002	0.12
ENSMUSG00000018983	*E2f2*	Transcription factor E2F2	-1.16	0.0006	0.13
ENSMUSG00000058290	*Espl1*	Separin	-1.21	0.0207	0.28
ENSMUSG00000015312	*Gadd45b*	Growth arrest and DNA damage-inducible protein GADD45 beta	2.06	0.0004	0.02
ENSMUSG00000021453	*Gadd45g*	Growth arrest and DNA damage-inducible protein GADD45 gamma	2.83	0.0006	0.01
ENSMUSG00000019777	*Hdac2*	Histone deacetylase 2	-1.17	0.0146	0.00
ENSMUSG00000029910	*Mad2l1*	Mitotic spindle assembly checkpoint protein MAD2A	-2.01	0.0011	0.06
ENSMUSG00000002870	*Mcm2*	DNA replication licensing factor MCM2	-2.74	0.0003	0.02
ENSMUSG00000041859	*Mcm3*	DNA replication licensing factor MCM3	-2.56	0.0010	0.06
ENSMUSG00000022673	*Mcm4*	DNA replication licensing factor MCM4	-2.23	0.0002	0.05
ENSMUSG00000005410	*Mcm5*	DNA replication licensing factor MCM5	-2.94	0.0004	0.03
ENSMUSG00000026355	*Mcm6*	DNA replication licensing factor MCM6	-1.45	0.0005	0.04
ENSMUSG00000029730	*Mcm7*	DNA replication licensing factor MCM7	-1.87	0.0021	0.06
ENSMUSG00000022346	*Myc*	Myc proto-oncogene protein	2.22	0.0004	0.07
ENSMUSG00000027342	*Pcna*	Proliferating cell nuclear antigen	-1.69	0.0003	0.03
ENSMUSG00000030867	*Plk1*	Serine/threonine-protein kinase PLK1	-3.36	0.0009	0.04
ENSMUSG00000022314	*Rad21*	Double-strand-break repair protein rad21 homolog	-1.04	0.0005	0.02
ENSMUSG00000027641	*Rbl1*	Retinoblastoma-like protein 1	-1.13	0.0074	0.10
ENSMUSG00000031666	*Rbl2*	Retinoblastoma-like protein 2	1.31	0.0029	0.10
ENSMUSG00000054115	*Skp2*	S-phase kinase-associated protein 2	-2.45	0.0003	0.16
ENSMUSG00000032402	*Smad3*	Mothers against decapentaplegic homolog 3	-1.17	0.0003	
ENSMUSG00000024974	*Smc3*	Structural maintenance of chromosomes protein 3	-1.16	0.0010	0.00

(Continued)

Table 2. Continued.

ENSEMBL ID	Gene symbol	Gene name	Log_2 Fold-change (DKO vs. WT)	FDR	dN/dS
ENSMUSG00000039239	*Tgfb2*	Transforming growth factor beta-2	-1.53	0.0234	0.04
ENSMUSG00000038379	*Ttk*	Dual specificity protein kinase TTK	-2.28	0.0008	0.24
ECM–receptor interaction: KEGG ID 4512					
ENSMUSG00000005087	*Cd44*	CD44 antigen	2.09	0.0177	0.42
ENSMUSG00000055447	*Cd47*	CD47 antigen (Rh-related antigen, integrin-associated signal transducer)	1.52	0.0009	0.36
ENSMUSG00000039084	*Chad*	chondroadherin	1.41	0.0189	0.03
ENSMUSG00000027966	*Col11a1*	collagen, type XI, alpha 1	-3.54	0.0009	0.06
ENSMUSG00000024330	*Col11a2*	collagen, type XI, alpha 2	-3.08	0.0010	0.08
ENSMUSG00000001506	*Col1a1*	collagen, type I, alpha 1	-2.54	0.0007	0.19
ENSMUSG00000029661	*Col1a2*	collagen, type I, alpha 2	-2.18	0.0003	0.16
ENSMUSG00000022483	*Col2a1*	collagen, type II, alpha 1	-5.79	0.0001	0.08
ENSMUSG00000026043	*Col3a1*	collagen, type III, alpha 1	-2.79	0.0004	0.14
ENSMUSG00000031502	*Col4a1*	collagen, type IV, alpha 1	1.61	0.0058	0.09
ENSMUSG00000031503	*Col4a2*	collagen, type IV, alpha 2	1.66	0.0066	0.18
ENSMUSG00000031273	*Col4a6*	collagen, type IV, alpha 6	-2.08	0.0052	0.32
ENSMUSG00000026837	*Col5a1*	collagen, type V, alpha 1	-1.26	0.0005	0.06
ENSMUSG00000026042	*Col5a2*	collagen, type V, alpha 2	-1.21	0.0037	0.06
ENSMUSG00000001119	*Col6a1*	collagen, type VI, alpha 1	1.73	0.0037	0.05
ENSMUSG00000020241	*Col6a2*	collagen, type VI, alpha 2	1.85	0.0195	0.06
ENSMUSG00000031849	*Comp*	cartilage oligomeric matrix protein	3.69	0.0026	0.04
ENSMUSG00000039952	*Dag1*	dystroglycan 1	1.14	0.0207	0.07
ENSMUSG00000020330	*Hmmr*	hyaluronan mediated motility receptor (RHAMM)	-3.10	0.0001	0.21
ENSMUSG00000090210	*Itga10*	integrin, alpha 10	2.17	0.0008	0.17
ENSMUSG00000001507	*Itga3*	integrin alpha 3	1.71	0.0001	0.13
ENSMUSG00000020689	*Itgb3*	integrin beta 3	1.13	0.0089	.07314/.09104
ENSMUSG00000020758	*Itgb4*	integrin beta 4	1.80	0.0032	0.07
ENSMUSG00000026971	*Itgb6*	integrin beta 6	1.11	0.0352	0.09
ENSMUSG00000001281	*Itgb7*	integrin beta 7	1.30	0.0036	0.12
ENSMUSG00000025321	*Itgb8*	integrin beta 8	1.14	0.0021	0.14
ENSMUSG00000015647	*Lama5*	laminin, alpha 5	1.26	0.0063	0.12
ENSMUSG00000002900	*Lamb1*	laminin B1	-1.12	0.0059	0.06
ENSMUSG00000026479	*Lamc2*	laminin, gamma 2	2.76	0.0123	0.18
ENSMUSG00000020592	*Sdc1*	syndecan 1	-1.88	0.0095	0.27
ENSMUSG00000022261	*Sdc2*	syndecan 2	1.11	0.0138	0.19
ENSMUSG00000017009	*Sdc4*	syndecan 4	1.44	0.0009	0.15
ENSMUSG00000029304	*Spp1*	secreted phosphoprotein 1	3.11	0.0236	0.29
ENSMUSG00000040152	*Thbs1*	thrombospondin 1	1.51	0.0263	0.04
ENSMUSG00000033327	*Tnxb*	tenascin XB	3.15	0.0034	0.11
ENSMUSG00000017344	*Vtn*	vitronectin	-1.12	0.0213	0.21
Complement and coagulation cascades: KEGG ID 4610					
ENSMUSG00000021070	*Bdkrb2*	B2 bradykinin receptor	1.10	0.0269	0.09
ENSMUSG00000036887	*C1qa*	Complement C1q subcomponent subunit A	1.78	0.0009	0.20
ENSMUSG00000036905	*C1qb*	Complement C1q subcomponent subunit B	1.00	0.0015	0.15
ENSMUSG00000036896	*C1qc*	Complement C1q subcomponent subunit C	1.20	0.0007	0.14
ENSMUSG00000055172	*C1ra*	Complement C1r-A subcomponent	2.65	0.0002	0.19
ENSMUSG00000024371	*C2*	Complement C2	2.24	0.0016	0.21
ENSMUSG00000024164	*C3*	Complement C3	2.73	0.0111	0.14
ENSMUSG00000029656	*C8b*	Complement component C8 beta chain	2.46	0.0007	0.23
ENSMUSG00000022149	*C9*	Complement component C9	-3.34	0.0000	0.35
ENSMUSG00000026399	*Cd55*	Complement decay-accelerating factor, GPI-anchored	1.70	0.0013	0.54
ENSMUSG00000090231	*Cfb*	Complement factor B	-1.45	0.0116	.16816/.16809
ENSMUSG00000021999	*Cpb2*	Carboxypeptidase B2	-1.31	0.0055	0.20

(Continued)

Table 2. Continued.

ENSEMBL ID	Gene symbol	Gene name	Log_2 Fold-change (DKO vs. WT)	FDR	d*N*/d*S*
ENSMUSG00000016481	*Cr1l*	Complement component receptor 1-like protein	1.13	0.0001	0.53
ENSMUSG00000031444	*F10*	Coagulation factor X	-2.89	0.0016	0.10
ENSMUSG00000026368	*F13b*	Coagulation factor XIII B chain	-2.19	0.0006	0.19
ENSMUSG00000048376	*F2r*	Proteinase-activated receptor 1	1.46	0.0015	0.13
ENSMUSG00000028128	*F3*	Tissue factor	2.56	0.0097	0.55
ENSMUSG00000033831	*Fgb*	Fibrinogen beta chain	1.36	0.0495	0.14
ENSMUSG00000022875	*Kng1*	Kininogen-1	1.57	0.0035	0.50
ENSMUSG00000028979	*Masp2*	Mannan-binding lectin serine protease 2	-1.09	0.0011	0.20
ENSMUSG00000024863	*Mbl2*	Mannose-binding protein C	-3.08	0.0027	0.48
ENSMUSG00000046223	*Plaur*	Urokinase plasminogen activator surface receptor	2.86	0.0053	0.23
ENSMUSG00000059481	*Plg*	Plasminogen	-1.97	0.0021	0.16
ENSMUSG00000024386	*Proc*	Vitamin K-dependent protein C	2.12	0.0008	0.17
ENSMUSG00000071177	*Serpina1d*	Alpha-1-antitrypsin 1–4	-1.48	0.0015	0.30
ENSMUSG00000072849	*Serpina1e*	Alpha-1-antitrypsin 1–5	2.52	0.0031	0.29
ENSMUSG00000041550	*Serpina5*	Plasma serine protease inhibitor	2.32	0.0370	0.25
ENSMUSG00000026715	*Serpinc1*	Antithrombin-III	-2.18	0.0005	0.11
ENSMUSG00000037411	*Serpine1*	Plasminogen activator inhibitor 1	1.91	0.0138	0.12
ENSMUSG00000038224	*Serpinf2*	Alpha-2-antiplasmin	-3.52	0.0002	0.27
ENSMUSG00000023224	*Serping1*	Plasma protease C1 inhibitor	2.21	0.0074	0.30

enriched in E18 DKO fetal membranes. Out of the 36 transcripts that were dysregulated in this pathway, 13 were collagens of different types, and nine different collagen transcripts were reduced in E18 DKO fetal membranes. These included *Col1a1*, *Col1a2*, *Col2a1*, *Col3a1*, *Col4a1*, *Col5a1*, *Col5a2*, *Col11a1*, and *Col11a2*.

PPROM is frequently associated with chorioamnionitis, an inflammation of fetal membranes that is associated with preterm birth [22]. Biglycan and decorin are degraded in most women experiencing severe chorioamnionitis at time of delivery [22]. Since chorioamnionitis is generally caused by bacterial infection, this again suggests a link between PPROM and bacterial infection, namely that infection impairs the ability for fetal tissues to regulate SLRPs in a way that ensures term gestation. In mice, it has previously been shown that the compensatory response of biglycan to a deficiency in decorin—and *vice versa*—is not present after infection and subsequent inflammation of expecting dams [26]. LPS and *E. coli* have been frequently used in mice to model infection-induced preterm birth, of which inflammation is a primary component [28]. One study investigated the effect of *E. coli* injection at E15 in single knockout $Bgn^{+/-}$; $Dcn^{-/-}$ and $Bgn^{-/-}$; $Dcn^{+/-}$ dams [26]. Days to delivery were reduced in $Bgn^{+/-}$; $Dcn^{-/-}$ and $Bgn^{-/-}$; $Dcn^{+/-}$ dams injected with *E. coli* and no live births resulted [26]. The authors suggest that "biglycan and decorin compensate for each other but lose the ability to do so under inflammation," causing decreased latency to preterm birth. It is therefore possible that presence of either biglycan or decorin may prevent inflammatory mechanisms in preterm birth, but loss of both exacerbates inflammation. The complement and coagulation cascade also play a key role in inflammation and immune responses. Our transcriptomic analysis showed upregulation of transcripts *C1qa*, *C1qb*, *C1qc*, *C1ra*, *C2*, and *C3* in E18 DKO fetal membranes. Human recombinant biglycan and decorin bind to complement C1q via both collagen and globular domains, preventing the classical pathway of complement activation, and inhibit binding of C1q to endothelial and U937 cells [67]. In women, activation of the C3a fragment of the complement cascade early during pregnancy is associated with increased risk for preterm membrane rupture [68]. Complement C1q and C3 are, therefore, ideal targets to investigate in E18 fetal membranes following DKO due to their putative role in PPROM in humans.

The 117 differentially expressed transcripts in the top three molecular pathways (cell cycle, complement cascade, and extracellular-matrix interaction) that were enriched in mouse fetal membranes at E18 following DKO exhibited $\omega < 1$, indicating that these genes are under purifying or negative selection pressure such that non-synonymous nucleotide substitutions are rarely tolerated. The functions of these genes are, therefore, likely conserved between the mouse and human, and these transcriptional changes may be translated from the mouse to the human. oPOSSUM-3 is a webtool that utilizes phylogenetic footprinting methods [44] to identify TFBS in conserved regulatory regions of genes in multiple species alignments. Using oPOSSUM-3, we have identified that 47 of the 117 genes in the cell cycle, complement cascade, and ECM-interaction that were differentially expressed following double knockout at E18 in mouse fetal membranes were enriched for transcription factor motifs for *Nr2f1* (nuclear receptor subfamily 2, group F, member 1).

Nr2f1, also known as COUP-transcription factor-1 (COUP-TF1), is a nuclear hormone receptor and transcription regulator, and mutations or deletions in this gene lead to Bosch–Boonstra-Schaaf optic atrophy associated with cerebral visual impairment and intellectual disability [69]. Chromatin immunoprecipitation-sequencing (ChIP-Seq) has been conducted to identify transcription factor binding sites of *Nr2f1* in human lymphoblast cell lines [70]. The identification of TFBS for *Nr2f1* following $Bgn^{-/-}$; $Dcn^{-/-}$ in mouse fetal membranes at E18 opens up avenues to further investigate the effect of loss of *Nr2f1* on fetal membranes using ChIP-Seq in this mouse model. Downregulation of *Nr2f1* and its target genes may be responsible for the profound effect of biglycan and decorin DKO on fetal membranes at E18 that resulted in the altered expression of 3264 transcripts compared to WT at this gestational stage.

Table 3. The 117 differentially expressed transcripts in the top three molecular pathways in mouse fetal membranes were enriched for regulatory motifs targeted by 13 transcription factors that were also differentially regulated following DKO of biglycan and decorin at E18 (FDR < 0.01).

ENSEMBL ID	Gene symbol	Gene name	log_2-FC (E18 WT vs. E18 KO)	FDR	JASPAR ID	Class	GC Content	Target gene hits	Target gene non-hits	Target TFBS hits	Target TFBS nucleotide rate	*Z*-score	Fisher score
ENSMUSG00000069171	*Nr2f1*	nuclear receptor subfamily 2, group F, member 1	-1.04	0.0122	MA0017.1	Zinc-coordinating	0.48	47	71	69	0.00298	10.347	8.768
ENSMUSG00000022952	*Runx1*	runt related transcription factor 1	1.45	0.0005	MA0002.2	Ig-fold	0.50	112	6	646	0.0219	6.989	18.758
ENSMUSG00000031627	*Irf2*	interferon regulatory factor 2	1.23	0.0017	MA0051.1	Winged Helix-Turn-Helix	0.41	11	107	11	0.000611	5.72	3.57
ENSMUSG00000022346	*Myc*	myelocytomatosis oncogene	2.22	0.0004	MA0147.1	Zipper-Type	0.69	68	50	173	0.00534	4.626	5.842
ENSMUSG00000037025	*Foxa2*	forkhead box A2	1.50	0.0062	MA0047.2	Winged Helix-Turn-Helix	0.32	99	19	406	0.015	3.919	9.973
ENSMUSG00000038418	*Egr1*	early growth response 1	1.16	0.0201	MA0162.1	Zinc-coordinating	0.74	49	69	86	0.00292	2.198	5.439
ENSMUSG00000038415	*Foxq1*	forkhead box Q1	2.54	0.0019	MA0040.1	Winged Helix-Turn-Helix	0.20	76	42	181	0.00615	0.523	8.28
ENSMUSG00000021255	*Esrrb*	estrogen related receptor, beta	-1.05	0.0175	MA0141.1	Zinc-coordinating	0.52	85	33	260	0.00963	-0.325	5.849
ENSMUSG00000026436	*Elk4*	ELK4, member of ETS oncogene family	1.15	0.0044	MA0076.1	Winged Helix-Turn-Helix	0.58	51	67	82	0.00228	-0.765	3.77
ENSMUSG00000027490	*E2f1*	E2F transcription factor 1	-2.11	0.0002	MA0024.1	Winged Helix-Turn-Helix	0.63	63	55	131	0.00324	-0.814	5.052
ENSMUSG00000000567	*Sox9*	SRY (sex determining region Y)-box 9	-1.53	0.0218	MA0077.1	Other Alpha-Helix	0.36	97	21	353	0.00981	-4.002	8.624
ENSMUSG00000039476	*Prrx2*	paired related homeobox 2	-1.34	0.0017	MA0075.1	Helix-Turn-Helix	0.03	107	11	894	0.0138	-5.235	7.28
ENSMUSG00000056749	*Nfil3*	nuclear factor, interleukin 3, regulated	1.93	0.0037	MA0025.1	Zipper-Type	0.27	55	63	103	0.0035	-6.721	2.143

Importantly, NR2F1 is expressed in human chorionic trophoblast progenitor cells, which have been described as a progenitor niche in the placenta, capable of differentiating into cytotrophoblasts and syncytiotrophoblast [71]. NR2F1 expression in colonies of human chorionic trophoblast progenitor cells may be required for self-renewal or differentiation [71]. Downregulation of *Nr2f1* in fetal membranes at E18 following double knockout of biglycan and decorin may therefore play a role not only by affecting downstream target binding sites, but also by affecting trophoblast differentiation in this mouse model. NR2F1 has been shown to be regulated by retinoic acid [72] and retinoid exposure (i.e., acne drug treatment) in pregnant women results in a variety of developmental defects and embryopathies [73].

In this study, we have utilized a mouse model of spontaneous preterm birth following double knockout of biglycan and decorin to investigate mechanisms by which membrane rupture and preterm birth may occur. We have identified three key molecular pathways, including cell cycle regulation, ECM–receptor interaction, and the complement and coagulation cascades that were altered in fetal membranes due to the double knockout of biglycan and decorin at E18. We speculate that that loss of the ECM proteins biglycan and decorin causes profound changes in the transcriptomic profile of fetal membranes throughout gestation, possibly leading to cell cycle suppression and complement activation, lack of proliferation of fetal membrane mesenchymal cells, and ultimately loss of membrane integrity and preterm birth in this mouse model. A key limitation to this study is that the exact mode of preterm birth cannot be absolutely described as PPROM due to the complex phenotype of this double knockout model but may also be due to cervical insufficiency or uterine dystocia. Another limitation to this study, as with any mouse model of preterm birth, is that mice have multiple pups in each litter (4–10 depending on the strain) [28], while humans do not, and twin pregnancies pose higher risk for preterm birth [4]. Despite these limitations, further studies using this model might provide insights into the various mechanisms of preterm birth. Future functional experiments will be necessary to validate these findings, and one promising approach involves the use of live cell imaging of CRISPR-Cas9 modified embryonic NIH/3T3 cells to investigate suppression of the cell-cycle [74]. Transcriptomic analysis of additional time points such as E15 will also provide a more holistic view of the changes occurring in fetal membranes throughout pregnancy in this mouse model.

Supplementary material

Supplementary material is available at *BIOLRE* online.

Acknowledgments

We would like to thank Dr. Alvaro Hernandez, Director of the High-Throughput Sequencing and Genotyping Unit, for his contribution in conducting the RNA-Seq at the Roy J. Carver Biotechnology Center, and Dr. Maria Carmen Valero Quiros for her contribution conducting the RNA extractions from mouse fetal membranes at the Carl R. Woese Institute for Genomic Biology, University of Illinois at Urbana-Champaign. Thomas Keller (University of South Florida) provided insightful comments on a draft of this manuscript.

Conflict of interest

The authors have declared that no conflict of interest exists.

References

1. Beck S, Wojdyla D, Say L, Betran AP, Merialdi M, Requejo JH, Rubens C, Menon R, Van Look PF. The worldwide incidence of preterm birth: a systematic review of maternal mortality and morbidity. *Bull World Health Organ* 2010; **88**:31–38.
2. Martin JA, Hamilton BE, Ventura SJ, Osterman MJ, Kirmeyer S, Mathews TJ, Wilson EC. Births: final data for 2009. *Natl Vital Stat Rep* 2011; **60**:1–70.
3. Romero R, Mazor M, Munoz H, Gomez R, Galasso M, Sherer DM. The preterm labor syndrome. *Human Endometrium* 1994; **734**:414–429.
4. Goldenberg RL, Culhane JF, Iams JD, Romero R. Epidemiology and causes of preterm birth. *Lancet* 2008; **371**:75–84.
5. Bouchet N, Joal A, Gayet-Ageron A, Areta ML, Martinez de Tejada B. Impact of the new guidelines on the management of premature rupture of membranes for the prevention of late preterm birth: an 11-year retrospective study. *J Perinat Med* 2019; **47**:341–346.
6. Mercer BM, Crocker LG, Pierce WF, Sibai BM. Clinical characteristics and outcome of twin gestation complicated by preterm premature rupture of the membranes. *Am J Obstet Gynecol* 1993; **168**:1467–1473.
7. Teodoro WR, Andreucci D, Palma JA. Short communication: placental collagen and premature rupture of fetal membranes. *Placenta* 1990; **11**:549–551.
8. Andreucci D, Cossermelli W, Rosolia WP, Pinto MN. The low hydroxyproline content of prematurely ruptured human fetal membranes. *Braz J Med Biol Res* 1986; **19**:351–354.
9. Evaldson GR, Larsson B, Jiborn H. Is the collagen content reduced when the fetal membranes rupture? A clinical study of term and prematurely ruptured membranes. *Gynecol Obstet Invest* 1987; **24**:92–94.
10. Meinert M, Eriksen GV, Petersen AC, Helmig RB, Laurent C, Uldbjerg N, Malmstrom A. Proteoglycans and hyaluronan in human fetal membranes. *Am J Obstet Gynecol* 2001; **184**:679–685.
11. Karamanos NK, Piperigkou Z, Theocharis AD, Watanabe H, Franchi M, Baud S, Brezillon S, Gotte M, Passi A, Vigetti D, Ricard-Blum S, Sanderson RD et al. Proteoglycan chemical diversity drives multifunctional cell regulation and therapeutics. *Chem Rev* 2018; **118**:9152–9232.
12. Meinert M, Malmstrom A, Tufvesson E, Westergren-Thorsson G, Petersen AC, Laurent C, Uldbjerg N, Eriksen GV. Labour induces increased concentrations of biglycan and hyaluronan in human fetal membranes. *Placenta* 2007; **28**:482–486.
13. Robinson KA, Sun M, Barnum CE, Weiss SN, Huegel J, Shetye SS, Lin L, Saez D, Adams SM, Iozzo RV, Soslowsky LJ, Birk DE. Decorin and biglycan are necessary for maintaining collagen fibril structure, fiber realignment, and mechanical properties of mature tendons. *Matrix Biol* 2017; **64**:81–93.
14. Gubbiotti MA, Vallet SD, Ricard-Blum S, Iozzo RV. Decorin interacting network: a comprehensive analysis of decorin-binding partners and their versatile functions. *Matrix Biol* 2016; **55**:7–21.
15. Hjelm AM, Barchan K, Malmstrom A, Ekman-Ordeberg GE. Changes of the uterine proteoglycan distribution at term pregnancy and during labour. *Eur J Obstet Gynecol Reprod Biol* 2002; **100**:146–151.
16. Faiyaz-Ul-Haque M, Zaidi SHE, Al-Mureikhi MS, Kennedy S, Al-Thani G, Tsui LC, Teebi AS. A novel missense mutation in the galactosyltransferase-I (B4GALT7) gene in a family exhibiting facioskeletal anomalies and Ehlers-Danlos syndrome resembling the progeroid type. *Am J Med Genet A* 2004; **128a**:39–45.
17. Yen JL, Lin SP, Chen MR, Niu DM. Clinical features of Ehlers-Danlos syndrome. *J Formos Med Assoc* 2006; **105**:475–480.
18. Schaefer L, Iozzo RV. Biological functions of the small leucine-rich proteoglycans: from genetics to signal transduction. *J Biol Chem* 2008; **283**:21305–21309.
19. Barabas AP. Ehlers-Danlos syndrome—associated with prematurity and premature rupture of foetal membranes—possible increase in incidence. *Br Med J* 1966; **2**:682–684.
20. Horgan CE, Roumimper H, Tucker R, Lechner BE. Altered decorin and Smad expression in human fetal membranes in PPROM. *Biol Reprod* 2014; **91**:1–7.

21. Hermanns-Le T, Pierard G, Quatresooz P. Ehlers-Danlos-like dermal abnormalities in women with recurrent preterm premature rupture of fetal membranes. *Am J Dermatopathol* 2005; **27**:407–410.
22. Meinert M, Malmstrom A, Petersen AC, Eriksen GV, Uldbjerg N. Chorioamniontis in preterm delivery is associated with degradation of decorin and biglycan and depletion of hyaluronan in fetal membranes. *Placenta* 2014; **35**:546–551.
23. Calmus ML, Macksoud EE, Tucker R, Iozzo RV, Lechner BE. A mouse model of spontaneous preterm birth based on the genetic ablation of biglycan and decorin. *Reproduction* 2011; **142**:183–194.
24. Nallasamy S, Yoshida K, Akins M, Myers K, Iozzo R, Mahendroo M. Steroid hormones are key modulators of tissue mechanical function via regulation of collagen and elastic Fibers. *Endocrinology* 2017; **158**:950–962.
25. Wu Z, Aron AW, Macksoud EE, Iozzo RV, Hai CM, Lechner BE. Uterine dysfunction in biglycan and decorin deficient mice leads to dystocia during parturition. *PLoS One* 2012; **7**:e29627.
26. de Araujo LBD, Horgan CE, Aron A, Iozzo RV, Lechner BE. Compensatory Fetal membrane mechanisms between biglycan and decorin in inflammation. *Mol Reprod Dev* 2015; **82**:387–396.
27. Iozzo RV, Schaefer L. Proteoglycan form and function: a comprehensive nomenclature of proteoglycans. *Matrix Biol* 2015; **42**:11–55.
28. McCarthy R, Martin-Fairey C, Sojka DK, Herzog ED, Jungheim ES, Stout MJ, Fay JC, Mahendroo M, Reese J, Herington JL, Plosa EJ, Shelton EL et al. Mouse models of preterm birth: suggested assessment and reporting guidelines. *Biol Reprod* 2018; **99**:922–937.
29. Goldenberg RL, Hauth JC, Andrews WW. Intrauterine infection and preterm delivery. *N Engl J Med* 2000; **342**:1500–1507.
30. Sanches JC, Jones CJ, Aplin JD, Iozzo RV, Zorn TM, Oliveira SF. Collagen fibril organization in the pregnant endometrium of decorin-deficient mice. *J Anat* 2010; **216**:144–155.
31. Xu TS, Bianco P, Fisher LW, Longenecker G, Smith E, Goldstein S, Bonadio J, Boskey A, Heegaard AM, Sommer B, Satomura K, Dominguez P et al. Targeted disruption of the biglycan gene leads to an osteoporosis-like phenotype in mice. *Nat Genet* 1998; **20**:78–82.
32. Danielson KG, Baribault H, Holmes DF, Graham H, Kadler KE, Iozzo RV. Targeted disruption of decorin leads to abnormal collagen fibril morphology and skin fragility. *J Cell Biol* 1997; **136**:729–743.
33. Wu Z, Horgan CE, Carr O, Owens RT, Iozzo RV, Lechner BE. Biglycan and decorin differentially regulate signaling in the fetal membranes. *Matrix Biol* 2014; **35**:266–275.
34. Bolger AM, Lohse M, Usadel B. Trimmomatic: a flexible trimmer for illumina sequence data. *Bioinformatics* 2014; **30**:2114–2120.
35. Ewels P, Magnusson M, Lundin S, Kaller M. MultiQC: summarize analysis results for multiple tools and samples in a single report. *Bioinformatics* 2016; **32**:3047–3048.
36. Armstrong DL, McGowen MR, Weckle Q, Pantham P, Caravas J, Agnew D, Benirschke K, Savage-Rumbaugh S, Nevo E, Kim JC, Wagner GP, Romero R, Wildman DE. The core transcriptome of mammalian placentas and the divergence of expression with placental shape. *Placenta* 2017; **57**:71–78.
37. Dobin A, Gingeras TR. Mapping RNA-seq reads with STAR. *Curr Protoc Bioinformatics* 2015; **51**:11-14–11-19.
38. Liao Y, Smyth GK, Shi W. The subread aligner: fast, accurate and scalable read mapping by seed-and-vote. *Nucleic Acids Res* 2013; **41**.
39. Liao Y, Smyth GK, Shi W. featureCounts: an efficient general purpose program for assigning sequence reads to genomic features. *Bioinformatics* 2014; **30**:923–930.
40. Robinson MD, McCarthy DJ, Smyth GK. edgeR: a Bioconductor package for differential expression analysis of digital gene expression data. *Bioinformatics* 2010; **26**:139–140.
41. Ritchie ME, Phipson B, Wu D, Hu YF, Law CW, Shi W, Smyth GK. Limma powers differential expression analyses for RNA-sequencing and microarray studies. *Nucleic Acids Res* 2015; **43**.
42. Luo W, Brouwer C. Pathview: an R/bioconductor package for pathway-based data integration and visualization. *Bioinformatics* 2013; **29**:1830–1831.
43. Falcon S, Gentleman R. Using GOstats to test gene lists for GO term association. *Bioinformatics* 2007; **23**:257–258.
44. Kwon AT, Arenillas DJ, Worsley Hunt R, Wasserman WW. oPOSSUM-3: advanced analysis of regulatory motif over-representation across genes or ChIP-Seq datasets. *G3 (Bethesda)* 2012; **2**:987–1002.
45. Buckberry S, Bianco-Miotto T, Bent SJ, Clifton V, Shoubridge C, Shankar K, Roberts CT. Placental transcriptome co-expression analysis reveals conserved regulatory programs across gestation. *BMC Genomics* 2017; **18**:10.
46. Sui SJH, Fulton DL, Arenillas DJ, Kwon AT, Wasserman WW. oPOSSUM: integrated tools for analysis of regulatory motif over-representation. *Nucleic Acids Res* 2007; **35**:W245–W252.
47. Yang Z, Nielsen R. Synonymous and nonsynonymous rate variation in nuclear genes of mammals. *J Mol Evol* 1998; **46**:409–418.
48. Jeffares DC, Tomiczek B, Sojo V, dos Reis M. A beginners guide to estimating the non-synonymous to synonymous rate ratio of all protein-coding genes in a genome. In: Peacock C. (eds) *Parasite Genomics Protocols. Methods in Molecular Biology*. New York, NY: Humana Press; 2015; vol. **1201**:65–90.
49. Stempfle G, McGowen MR, Caravas JA, Wildman DE. From PPROM to caul: the evolution of membrane rupture in mammals. *Appl Transl Genom* 2013; **2**:70–77.
50. Yang Z. PAML 4: phylogenetic analysis by maximum likelihood. *Mol Biol Evol* 2007; **24**:1586–1591.
51. Eidem HR, Ackerman WE, McGary KL, Abbot P, Rokas A. Gestational tissue transcriptomics in term and preterm human pregnancies: a systematic review and meta-analysis. *BMC Med Genomics* 2015; **8**:27.
52. Dobreva MP, Pereira PN, Deprest J, Zwijsen A. On the origin of amniotic stem cells: of mice and men. *Int J Dev Biol* 2010; **54**:761–777.
53. Pereira PN, Dobreva MP, Graham L, Huylebroeck D, Lawson KA, Zwijsen AN. Amnion formation in the mouse embryo: the single amniochorionic fold model. *BMC Dev Biol* 2011; **11**:48.
54. Nielsen BW, Bonney EA, Pearce BD, Donahue LR, Sarkar IN, Collaborative PBI. A cross-species analysis of animal models for the investigation of preterm birth mechanisms. *Reprod Sci* 2016; **23**:482–491.
55. O'Rahilly R, Muller F. Developmental stages in human embryos: revised and new measurements. *Cells Tissues Organs* 2010; **192**:73–84.
56. Theiler K. *The House Mouse: Atlas of Embryonic Development*, vol. **178**. New York: Springer-Verlag; 1989.
57. Blum JL, Chen LC, Zelikoff JT. Exposure to ambient particulate matter during specific gestational periods produces adverse obstetric consequences in mice. *Environ Health Perspect* 2017; **125**:077020.
58. Xing X, Gu X, Ma T. Knockdown of biglycan expression by RNA interference inhibits the proliferation and invasion of, and induces apoptosis in, the HCT116 colon cancer cell line. *Mol Med Rep* 2015; **12**:7538–7544.
59. Santra M, Mann DM, Mercer EW, Skorski T, Calabretta B, Iozzo RV. Ectopic expression of decorin protein core causes a generalized growth suppression in neoplastic cells of various histogenetic origin and requires endogenous p21, an inhibitor of cyclin-dependent kinases. *J Clin Investig* 1997; **100**:149–157.
60. DeGregori J, Johnson DG. Distinct and overlapping roles for E2F family members in transcription, proliferation and apoptosis. *Curr Mol Med* 2006; **6**:739–748.
61. Hildebrand A, Romaris M, Rasmussen LM, Heinegard D, Twardzik DR, Border WA, Ruoslahti E. Interaction of the small interstitial proteoglycans biglycan, decorin and fibromodulin with transforming growth factor beta. *Biochem J* 1994; **302**:527–534.
62. Kresse H, Schonherr E. Proteoglycans of the extracellular matrix and growth control. *J Cell Physiol* 2001; **189**:266–274.
63. Bassols A, Massague J. Transforming growth factor beta regulates the expression and structure of extracellular matrix chondroitin/dermatan sulfate proteoglycans. *J Biol Chem* 1988; **263**:3039–3045.
64. Yamaguchi Y, Mann DM, Ruoslahti E. Negative regulation of transforming growth factor-beta by the proteoglycan decorin. *Nature* 1990; **346**:281–284.
65. Liu Y, Beyer A, Aebersold R. On the dependency of cellular protein levels on mRNA abundance. *Cell* 2016; **165**:535–550.

66. Zhang G, Chen S, Goldoni S, Calder BW, Simpson HC, Owens RT, McQuillan DJ, Young MF, Iozzo RV, Birk DE. Genetic evidence for the coordinated regulation of collagen fibrillogenesis in the cornea by decorin and biglycan. *J Biol Chem* 2009; **284**:8888–8897.
67. Groeneveld TW, Oroszlan M, Owens RT, Faber-Krol MC, Bakker AC, Arlaud GJ, McQuillan DJ, Kishore U, Daha MR, Roos A. Interactions of the extracellular matrix proteoglycans decorin and biglycan with C1q and collectins. *J Immunol* 2005; **175**:4715–4723.
68. Lynch AM, Gibbs RS, Murphy JR, Giclas PC, Salmon JE, Holers VM. Early elevations of the complement activation fragment C3a and adverse pregnancy outcomes. *Obstet Gynecol* 2011; **117**:75–83.
69. Bosch DG, Boonstra FN, Gonzaga-Jauregui C, Xu M, de Ligt J, Jhangiani S, Wiszniewski W, Muzny DM, Yntema HG, Pfundt R, Vissers LE, Spruijt L et al. NR2F1 mutations cause optic atrophy with intellectual disability. *Am J Hum Genet* 2014; **94**:303–309.
70. Consortium EP. An integrated encyclopedia of DNA elements in the human genome. *Nature* 2012; **489**:57–74.
71. Genbacev O, Donne M, Kapidzic M, Gormley M, Lamb J, Gilmore J, Larocque N, Goldfien G, Zdravkovic T, McMaster MT, Fisher SJ. Establishment of human trophoblast progenitor cell lines from the chorion. *Stem Cells* 2011; **29**:1427–1436.
72. Love CE, Prince VE. Expression and retinoic acid regulation of the zebrafish nr2f orphan nuclear receptor genes. *Dev Dyn* 2012; **241**:1603–1615.
73. Browne H, Mason G, Tang T. Retinoids and pregnancy: an update. *Obstet Gynaecol* 2014; **16**:7–11.
74. Otsuka K, Tomita M. Concurrent live imaging of DNA double-strand break repair and cell-cycle progression by CRISPR/Cas9-mediated knock-in of a tricistronic vector. *Sci Rep* 2018; **8**: 17309.